Kinetic Analysis of the Pyrolysis of Phenethyl Phenyl Ether: Computational Prediction of α/β-Selectivities

Ariana Beste,*,† A. C. Buchanan III,‡ Phillip F. Britt,‡ Bryan C. Hathorn,† and Robert J. Harrison†

Computer Science and Mathematics Division, Oak Ridge National Laboratory, Bethel Valley Road, Oak Ridge, Tennessee 37831-6367, and Chemical Sciences Division, Oak Ridge National Laboratory, Bethel Valley Road, Oak Ridge, Tennessee 37831-6197

Received: July 25, 2007; In Final Form: September 19, 2007

We calculated an overall α/β-selectivity for the pyrolysis of phenethyl phenyl ether as a composite of the α/β-selectivities in the hydrogen abstraction reactions by the phenoxyl and by the benzyl radical that is in excellent agreement with experiment. The difference between the individual selectivities for these radicals is explained by analyzing the electronic structure of the transition states. Spin delocalization of the single electron favors the α-pathways. An opposing effect occurs for polarized transition states, such as the transition states for the hydrogen abstraction by the electrophilic phenoxyl radical, where the adjacent ether oxygen in phenethyl phenyl ether stabilizes the β-transition states. These results indicate that theory will be able to provide excellent predictions of α/β-product selectivities for more complicated lignin model compounds bearing multiple substituents. We have developed a scheme to predict α/β-product selectivities in the pyrolysis of model compounds for the β-ether linkage in lignin. The approach is based on computation of the relative rate constant, which profits from error cancellation in the individual rate constants. The Arrhenius prefactors depend strongly on the description of the low-frequency modes for which anharmonic contributions are important. We use density functional theory in combination with transition-state theory in this analysis. Diagonal anharmonic effects for individual low-frequency modes are included by employing a second-order Wigner−Kirkwood expansion in a semiclassical expression for the vibrational partition function. The composite α/β-product selectivity is obtained by applying quasi-steady-state kinetic analysis for the intermediate radicals.

Introduction

Lignin is found in the cell walls of vascular plants and is one of the most abundant organic compounds on earth after cellulose and chitin. The naturally occurring biopolymer is a potential source of oxygenated chemicals, such as phenols and sugars, and liquid fuels. Large amounts of lignin are available as a byproduct of the pulping process. Lignin is a complex, highly branched, three-dimensional polymer that is processed and analyzed[1−3] mainly through pyrolysis. Because the decomposition of lignin leads to a variety of products and bio-oils that need further refinement, the development of efficient processing techniques is an active area of recent research. Comprehensive reviews on the gasification and thermochemical conversion of biomass are available.[4−7]

The investigation of model compounds is a valuable tool to gain insight into the fundamental kinetic and mechanistic details of the reactions of the building blocks of lignin under the influence of heat. The dominant interunit linkage in lignin is the arylglycerol-β-aryl ether linkage shown in Figure 1. There have been many studies devoted to the pyrolysis of model compounds for the β-ether linkage.[8−12] The simplest model of the β-ether linkage in lignin is phenethyl phenyl ether (PPE).

Britt et al.[13] studied the thermal decomposition of PPE in liquid and gas phases and similar product selectivities were obtained in both cases. Different mechanisms for the thermolysis of PPE have been discussed.[14,15] Britt et al.[13] provided evidence for a free-radical chain mechanism in the temperature range 330−425 °C to explain formation of the primary products, $PhCH_3$, PhCHO, PhOH, and $PhCHCH_2$. The cracking of PPE proceeds through two competitive pathways, defined as α/β-selectivity, referring to the products derived from the hydrogen abstraction at the α- and β-position of PPE by chain carrying benzyl and phenoxyl radicals, as will be discussed in more detail below.

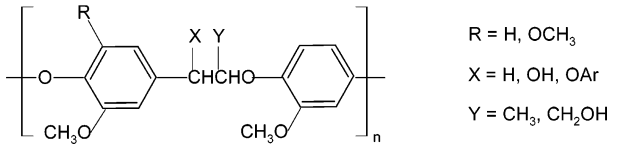

Figure 1. Arylglycerol-β-aryl ether linkage in lignin.

The average α/β-selectivity in the liquid and the gas phase was measured to be 3.1 ± 0.3 at 375 °C. Products derived from the radicals formed on the β-position were not expected to have such a high contribution because the radical formed at the benzylic α-position is more stable than the radical formed on the β-position by an estimated 7 kcal/mol.[13] The measured α/β-product selectivity is a composite of the individual hydrogen abstraction selectivities for both benzyl and phenoxyl radicals, which can only be crudely estimated for the benzyl radical from existing experimental data.[13] Kinetic data for hydrogen abstraction by phenoxyl radicals on hydrocarbons is difficult to access experimentally because of the rapid recombination of phenoxyl

* Corresponding author. E-mail: bestea@ornl.gov. Phone: 865-241-3160. Fax: 865-574-0680.
† Computer Science and Mathematics Division.
‡ Chemical Sciences Division.

10.1021/jp075861+ CCC: $37.00
Published on Web 11/09/2007

radicals. The current hypothesis to explain the unexpectedly low α/β-selectivity invokes polar effects in the hydrogen abstraction reaction by the electrophilic, chain carrying phenoxyl radical.[13] Hence, a central issue to understanding and predicting the reaction selectivity in lignin models is the ability to understand the rates of hydrogen abstraction at the α and β sites by both benzyl and phenoxyl radicals.

The computation of rate constants is a challenging task, in particular for large systems. Depending on the temperature, calculated absolute rate constants for hydrogen abstraction reactions can differ from experimental and otherwise calculated values by orders of magnitude with large uncertainties also present in the experimental rate constants.[16−20] Small errors in calculated activation energies (under 2 kcal/mol) and small changes in the prefactors (difference in log *A* smaller than 2) can change the absolute rate constant by an order of magnitude. Accurate absolute rate constants have been calculated for hydrogen abstraction reactions in small and rigid systems[21−25] using a high level of theory and variational transition-state theory based on the work of Truhlar and co-workers.[26,27]

However, we are interested in organic radical reactions where the molecule size makes it necessary to find a cost-effective but accurate way to provide kinetic data. Few computational studies have been done that investigate the kinetics of hydrogen abstraction reactions involving large molecules.[28−31] The importance of the correct treatment of the low-frequency modes that correspond to internal rotation[28,31] and the sensitivity to the choice of the large amplitude motion coordinate[32] has been pointed out. A particular difficulty in our systems is the occurrence of a large number of low-frequency modes; about nine frequencies per transition state are below 100 cm^{-1}. All of these modes are coupled and have large anharmonic contributions. The hindered rotor approximation on the other hand assumes that the large amplitude motion corresponding to the internal rotation is separable from the small amplitude vibrations.

Our computation protocol to determine the relative rate constant is consciously structured to cancel systematic errors in the individual rate constants. In particular, the α/β-selectivity is determined by the activation energies and partition functions of similar transition states, because the α and β pathways have the same reactants. We expect the error cancellation to work well for the activation energies. On the other hand, the vibrational partition functions and therefore the prefactors are very sensitive to the low-frequency modes. In fact, for related hydrogen abstraction reactions we recently observed spurious imaginary modes that are the consequence of exaggerated numerical errors in finite-difference calculations on a flat potential energy surface and the break down of the harmonic approximation.[33] For these modes the harmonic quantum partition functions cannot be calculated. Without the incorporation of anharmonic effects in the low-frequency modes, a systematic error cancellation is not expected for the prefactors.

Anharmonic corrections to vibrations can be calculated by solving the vibrational Schrödinger equation with perturbation theory[34] or with a self-consistent field method[35] where correlation effects between modes can be included.[35,36] The necessary anharmonic force field is commonly obtained by a finite-difference procedure for calculating anharmonic force constants from analytic second derivatives.[37] Variations of this method, depending on the availability of analytical derivatives, are applicable to high-level electronic structure methods[38] and density functional theory (DFT).[39] The calculated anharmonic frequencies and zero point energies (ZPE) can be used to calculate vibrational partition functions that include anharmonic effects but retain the formal expression of the harmonic partition function.[40]

However, we are not interested in the anharmonic frequencies themselves but only in the corrected vibrational partition functions. For the low-frequency modes, we therefore calculate the anharmonic partition functions directly. For high-frequency modes, which are described well by the harmonic approximation, we use the quantum harmonic partition function. Within the experimental temperature range explored, the low-frequency modes can be treated semiclassically. We calculate the anharmonic potential along each low-frequency normal mode numerically and use a Wigner−Kirkwood expansion[41] for the particle density in a semiclassical expression of the partition function. This enables us to include diagonal anharmonic effects for chosen normal modes to the precision to which we calculate the corresponding anharmonic potential. Using the anharmonic partition function for a single low-frequency mode to compute the vibrational partition of the transition state can result in a 20% correction in the absolute rate constant.

Our goal is to develop a predictive tool to compute the α/β-selectivity observed in the pyrolysis of substituted lignin model compounds by calculating reliable relative rate constants involving medium size molecules and radicals (in this work, up to 22 heavy atoms but not limited to this number). We use DFT in combination with transition-state theory[42] to calculate relative rate constants of very similar reactions. We include diagonal anharmonic corrections for low-frequency modes. Needed kinetic data to explain the observed α/β-selectivity in the pyrolysis of PPE are provided, and mechanistic insight is gained through the analysis of the electronic structure of the transition states involved.

Computational Details

All calculations were carried out with the NWChem program package.[43] We used unrestricted density functional methods to search for equilibrium and transition-state structures. There has been evidence that DFT, including the B3LYP functional,[44,45] underestimates the reaction barriers for hydrogen abstraction reactions.[46,47] Regardless, the B3LYP functional is used to study hydrogen abstraction reactions on medium size organic molecules.[48−50] In our work, the accurate determination of the reaction barrier is less important than the correct reproduction of trends. It has been suggested that the BHandHLYP[45,51] functional is superior to the B3LYP functional in calculating hydrogen abstraction barriers.[52,53] However, we studied hydrogen abstraction reactions similar to the hydrogen abstraction reactions occurring in the pyrolysis of PPE to calibrate electronic structure methods for this class of reactions. We found that the B3LYP functional predicts reaction barriers in agreement with experiment, whereas the BHandHLYP functional substantially underestimates the barriers, and the MP2 method overestimates them.[33] It has also been shown that the B3LYP functional computes anharmonic force constants well.[39] We therefore use the B3LYP functional to study the pyrolysis of PPE.

Additionally, for the hydrogen abstraction reaction on PPE by the phenoxyl radical, we employed the MPW1K functional[54] because it has been reported to give better reaction barriers for hydrogen abstraction reactions than the B3LYP functional and to be more suitable for kinetic studies.[31,55,56] The transition-state geometries obtained were similar to the ones calculated with the B3LYP functional, and the reaction barriers differed by an average of only 0.26 kcal/mol for the five investigated transition states. The reaction energies differed by 2.9 kcal/mol

for the α pathway and by 2.7 kcal/mol for the β pathway. However, reaction energies are not required to determine the α/β-selectivity and we report only B3LYP results throughout the paper.

The grid on which the exchange-correlation contribution to the density functional is evaluated was set to be extra fine, which gives an approximate accuracy of the total energy of 10^{-8} H. A mixed basis set was used for the geometry optimizations and frequency calculations. The mixed basis set consists of a 6-31G* basis for all atoms, except for the ones on which the unpaired electron is located; for these a 6-31++G** basis set was used. In the transition states, the 6-31++G** basis set was employed for the transferred hydrogen atom and the two neighboring atoms. In the equilibrium structures the carbon atoms in aromatic rings adjacent to the radical center were also treated with the 6-31++G** basis set. Single point calculations were performed for all stationary points using the 6-311++G** basis set on all atoms. Energy differences are zero point corrected. To verify the validity of the mixed basis set, we repeated all geometry optimization for the hydrogen abstraction on PPE by the phenoxyl radical with the 6-311++G** basis set. The reaction barriers for the five investigated transition states differed on average by only 0.26 kcal/mol.

We preoptimized the transition states for the hydrogen abstraction by the benzyl radical with a fixed hydrogen benzyl as well as a fixed hydrogen PPE distance. The transition states for the hydrogen abstraction by the phenoxyl radical were preoptimized with a fixed hydrogen phenoxyl as well as a fixed hydrogen PPE distance. To ensure that the conformational space is well sampled, we chose five starting structures per reaction distinguished by different orientations of the reactants to each other. We found multiple transition states in the saddle point search for all reactions investigated.

Rate Constants and the Wigner−Kirkwood Expansion

The rate constants are calculated with transition-state theory.[42] The rate of the reaction is determined by the rate of crossing of the barrier. We assume that the transition state is in equilibrium with the reactants and that all transition states are accessible from the ground electronic state. For the reactions considered in this work, we obtain multiple transition states for the same reaction, each one defining a reaction path. The rate constant is the sum over all reaction paths

$$k = \frac{k_B T}{h Q_R} \sum_i Q^{\#}_{TS_i} e^{-\Delta E_i/RT} \tag{1}$$

where k_B is the Boltzmann constant, R is the ideal gas constant, T is the temperature, h is the Planck constant, ΔE_i is the zero point corrected activation barrier through the ith transition state, and Q are the partition functions for the transition states (TS_i) and the reactants (R). The superscript # means that the vibration responsible for the dissociation of the transition state (the imaginary frequency) is taken out of the partition function. The molecular partition functions are a product of the partition functions for translational, vibrational, rotational, and electronic energy partition functions, where the electronic partition function is unity.

The harmonic approximation to the quantum partition function is given as

$$q_v = \prod_j \frac{e^{-\beta h \nu_j/2}}{1 - e^{-\beta h \nu_j}} \tag{2}$$

where ν_j is the frequency of the normal mode j and $\beta = 1/k_B T$. We use the harmonic quantum partition function for frequencies larger than 100 cm^{-1}; this choice is rationalized below.

Because of the exponential dependence of the harmonic vibrational partition function on the frequencies, low-frequency modes have a large contribution to the partition function. On the other hand, for small frequencies the anharmonic effects become increasingly important. Alternatively, an anharmonic vibrational potential can be incorporated into a semiclassical expression for the vibrational partition function. Within the experimental temperature range 600−700 K, a semiclassical expression of the partition function is appropriate for frequencies below 100 cm^{-1}, as will be demonstrated below. The semiclassical partition function is an integral over the particle density $\rho_\beta(x_j)$ as a function of the normal mode coordinate x_j

$$q_v = \int \rho_\beta(x_j)\, dx_j \tag{3}$$

We use a Wigner−Kirkwood perturbation expansion[41] of the particle density in terms of the small parameter λ, which is given as

$$\lambda = \frac{h^2 \beta^2}{8 \mu_j \pi^2} \tag{4}$$

where μ_j is the effective mass for mode j and is calculated as

$$\mu_j = \left(\sum_i^{3N} l_{i,j}^{\ 2} \right)^{-1} \tag{5}$$

The sum goes over the $3N$ coordinates and l is the vector of Cartesian displacement of the normal mode j. The second-order Wigner−Kirkwood expansion is written in terms of the classical particle density $\rho_\beta^{Cl}(x_j)$

$$\rho_\beta(x_j) = \rho_\beta^{Cl}(x_j)(1 + \lambda A_1 + \lambda^2 A_2) \tag{6}$$

The classical particle density is given by

$$\rho_\beta^{Cl} = h^{-1} \sqrt{\frac{2\pi\mu_j}{\beta}}\, e^{-\beta V(x_j)} \tag{7}$$

and the expansion coefficients are

$$A_1 = \frac{\beta}{12} (V')^2 - \frac{1}{6} V'' \tag{8}$$

$$A_2 = \frac{\beta^2}{288} (V')^4 - \frac{11\beta}{360} (V')^2 V'' + \frac{1}{40} (V'')^2 + \frac{1}{30} V' V''' - \frac{1}{60\beta} V^{IV} \tag{9}$$

The coefficients depend on the various derivatives of the potential $V(x_j)$, which is a function of the normal mode coordinate x_j. The potential $V(x_j)$ is a fourth-order polynomial fit to the potential obtained by displacing along mode j. Using an anharmonic potential along a normal mode in the calculation of the partition function allows for diagonal anharmonic corrections in the rate constants. The coupling between the modes is only included on the level of the harmonic approximation.

Results and Discussion

Britt et al.[10] concluded that the thermal decomposition of PPE proceeds through a free radical chain mechanism, which is

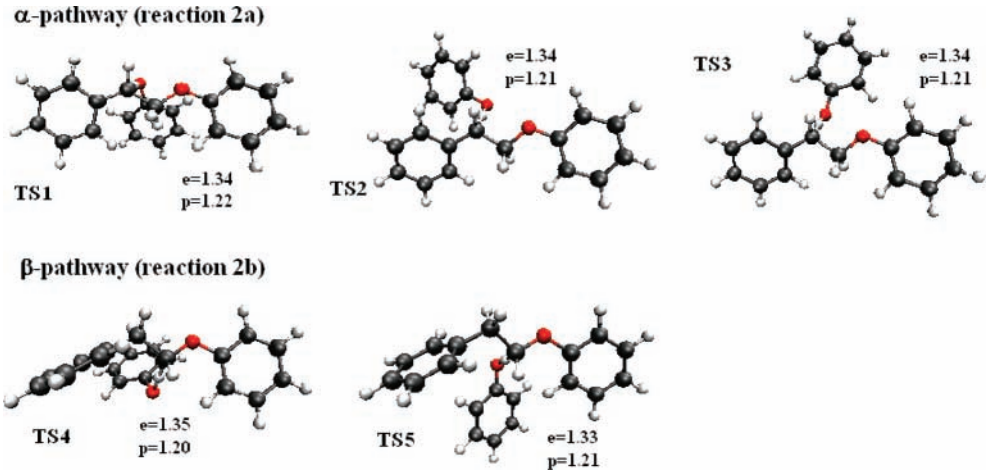

Figure 2. Transition-state geometries for hydrogen abstraction by phenoxyl radical (reaction 2): e, H-PPE bond lengths in Å; p, H-phenoxyl bond lengths in Å.

SCHEME 1: Radical Chain Mechanism for the Thermal Decomposition of PPE

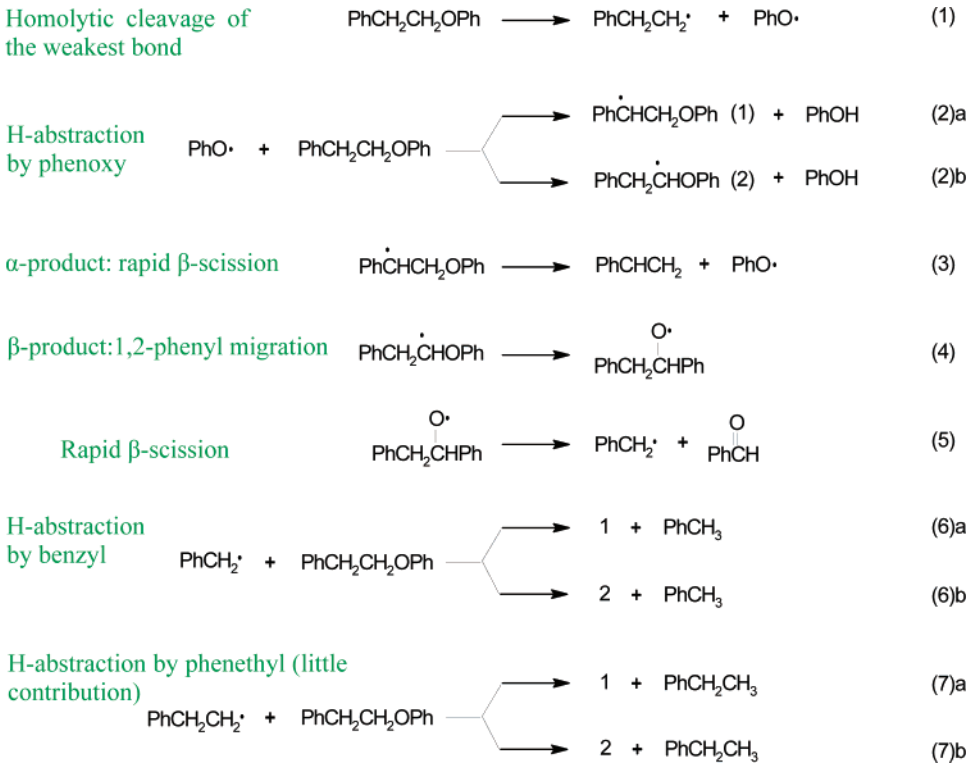

shown in Scheme 1. The initial step is the homolytic cleavage of the weakest bond in PPE (reaction 1), which is followed by hydrogen abstraction by the phenoxyl radical on the α- or *β*-position of PPE (reactions 2a and 2b). The hydrogen abstraction by the phenethyl radical (reactions 7a and 7b) has only a small contribution to the radical chain. The PPE α-radical, which is formed in reaction 2a, undergoes rapid *β*-scission (reaction 3) forming the chain carrying phenoxyl radical. The PPE *β*-radical, formed in reaction 2b, reacts further through 1,2 phenyl migration (reaction 4) to generate a radical that undergoes rapid *β*-scission (reaction 5) to form the second chain carrying radical, the benzyl radical. The benzyl radical also abstracts hydrogen competitively at the α- and *β*-position of PPE (reactions 6a and 6b).

The measured α/*β*-product selectivity is a composite of the α/*β*-selectivity of the hydrogen abstraction by the phenoxyl radical (reaction 2) and the α/*β*-selectivity of the hydrogen abstraction by the benzyl radical (reaction 6). To determine the contributions of these two selectivities to the overall α/*β*-selectivity, we therefore investigate in detail the four key reactions: reactions 2a, 2b, 6a, and 6b.

A. Electronic Structure Calculations. We found three transition states for the hydrogen abstraction by the phenoxyl radical on the α-position of PPE (reactions 2a) and two transition states for the hydrogen abstraction on the *β*-position of PPE (reaction 2b), which are shown in Figure 2. For each reaction the transition states differ by the position of the phenyl ring relative to PPE, which roughly corresponds to a rotation of the phenyl ring around the C−H−O axis along which the hydrogen atom is transferred. This observation suggests that the transition states are connected by a hindered rotation and could be combined into a single transition state by applying the hindered rotor approximation. However, each transition state has a large number of coupled low-frequency modes, which makes it extremely difficult to separate the internal rotation from the remaining low-frequency modes. We therefore assign a reaction

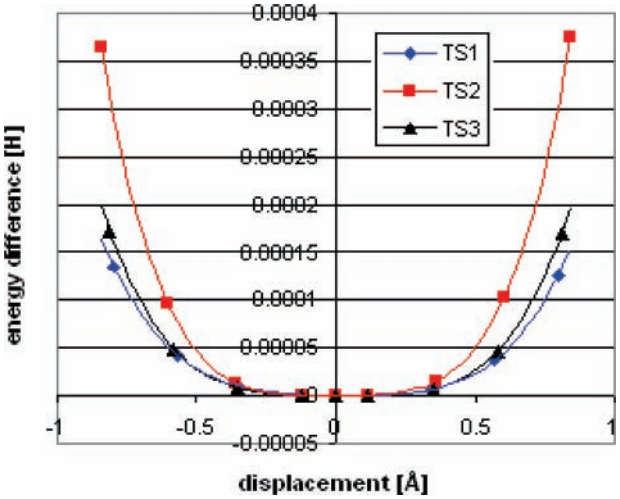

Figure 3. Potentials obtained by displacement along spurious imaginary modes in **TS1**, **TS2**, and **TS3**.

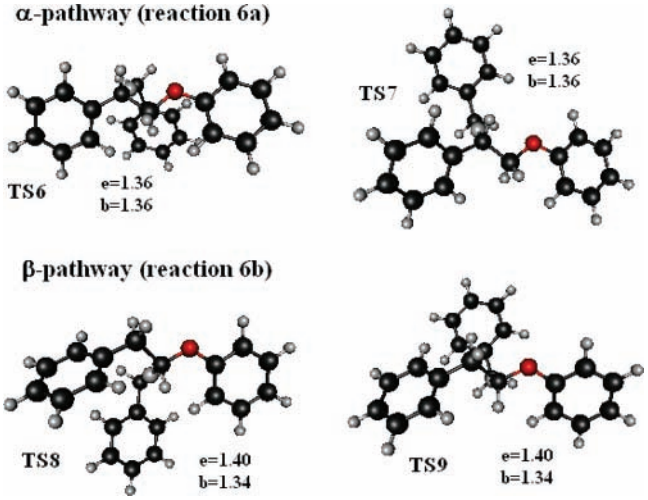

Figure 4. Transition-state geometries for hydrogen abstraction by benzyl radical (reaction 6): e, H-PPE bond lengths in Å; b, H-benzyl bond lengths in Å.

path to each transition state. In all transition states the transferred hydrogen atom is positioned closer to phenoxyl than it is to PPE, which indicates late transition states.

The vibrational analysis showed that the transition states in Figure 2 have a large imaginary frequency (~1800i cm^{-1}) corresponding to the displacement along reaction coordinate. For the transition states of the β-pathway this is the only imaginary frequency, but all three transition states of the α-pathway have a spurious imaginary frequency of 3.6i, 3.5i, and 7.3i cm^{-1} in **TS1**, **TS2**, and **TS3**, respectively. For similar hydrogen abstraction reactions, we have seen that spurious imaginary frequencies can occur not as a consequence of loose convergence criteria but because of numerical errors in the finite difference calculation of the second derivatives.[33] For very low frequencies these artifacts can cause the occurrence of imaginary modes. Figure 3 shows the potentials obtained by displacement along the spurious imaginary modes in **TS1**, **TS2**, and **TS3**. The lowest energies are seen to be at zero displacement. The fits to the potentials have large cubic and fourth-order coefficients; for example, the fit to the potential for **TS1** is $E = 0.0003x^4 - 3 \times 10^{-6}x^3 + 4 \times 10^{-5}x^2 - 4 \times 10^{-6}x - 2 \times 10^{-8}$. We use the anharmonic potentials obtained by displacement along the normal modes directly in eqs 7−9, which is discussed in the next section.

For the hydrogen abstraction on PPE by the benzyl radical (reaction 6), we also found multiple transition states for both pathways, which are given in Figure 4. Again, we see that the difference between the transition states is the relative position of the phenyl ring to PPE. The transition states for the α-pathway (reaction 6a) are symmetric in the sense that the distances from the transferred hydrogen atom to PPE and to benzyl are equal. In the transition states for the β-pathway (reaction 6b) the hydrogen−PPE bond is longer than the hydrogen−benzyl bond, as we have observed for the phenoxyl transition states. The vibrational analysis for the benzyl transition states recorded one imaginary frequency in each transition state.

Figure 5 shows the reaction profile for the hydrogen abstraction reaction on PPE by the phenoxyl radical (reaction 2) and the benzyl radical (reaction 6). The energy difference between the α-radical product and the β-radical product is 6.7 kcal/mol, consistent with the previous thermochemical kinetic prediction.[13] The α-radical is stabilized relative to the β-radical through delocalization of the single electron in the neighboring aromatic ring. The delocalization of the electron can be monitored by plotting the spin density (the difference between spin up and spin down density); see Figure 6. Because in the α-transition states the single electron could also be delocalized in the aromatic ring but not in the β-transition states, one could expect a similar energy difference between the α- and β-transition states. As Figure 5 shows, this difference is much smaller. In Figure 7, the spin densities for the lowest transition states of the α- and β-pathways for the phenoxyl and benzyl radical abstraction are depicted. Most of the spin density is located in the hydrogen bridge. Even though the stabilization through delocalization in the benzylic ring of the α-transition states is visible, it is much less pronounced in the transition states than in the product radicals.

Another observation we can make in Figure 5 is that there is only a very small barrier difference for the α- and β-pathways for the phenoxyl abstraction (0.3 kcal/mol) but there is a larger barrier difference for the benzyl abstraction (2.4 kcal/mol). To explain this, we look at the charge differences between the transition states and the reactants for the lowest transition states of the α- and β-pathways for the phenoxyl and the benzyl abstraction in Figure 8. The partial atomic charges are calculated by a fitting procedure of the quantum mechanical electrostatic potential on selected grid points. There is no increase in the total polarization when the benzyl transition states are formed. The system response is a local charge rearrangement. In particular, the ether oxygen participates with approximately the same amount of charge in the redistribution in the α- and in the β-transition state. On the other hand, the electrophilic attack of the phenoxyl radical causes the phenoxyl transition states to polarize; i.e., charge is drawn into the phenoxyl ring. In the α-transition state the PPE ether oxygen hardly donates any charge. In the β-transition states, however, the ether oxygen adjacent to the radical attack donates charge and stabilizes the polarized transition state. As a consequence, the barrier difference between α- and β-pathways caused by the stabilization through electron delocalization in the α-transition states decreases. The described effect is also known as a polar effect.[57]

B. Kinetic Analysis. For the four reactions studied (reactions 2a, 2b, 6a, 6b) we found in total nine transition states. Each transition state has nine harmonic frequencies, which are about 100 cm^{-1} or less. There is one frequency per transition state lower than 20 cm^{-1}. We calculated the anharmonic potentials for the smallest frequency in each transition state by displacing along the normal mode and fitting to a fourth-order polynomial. For the remaining eight frequencies per transition state we

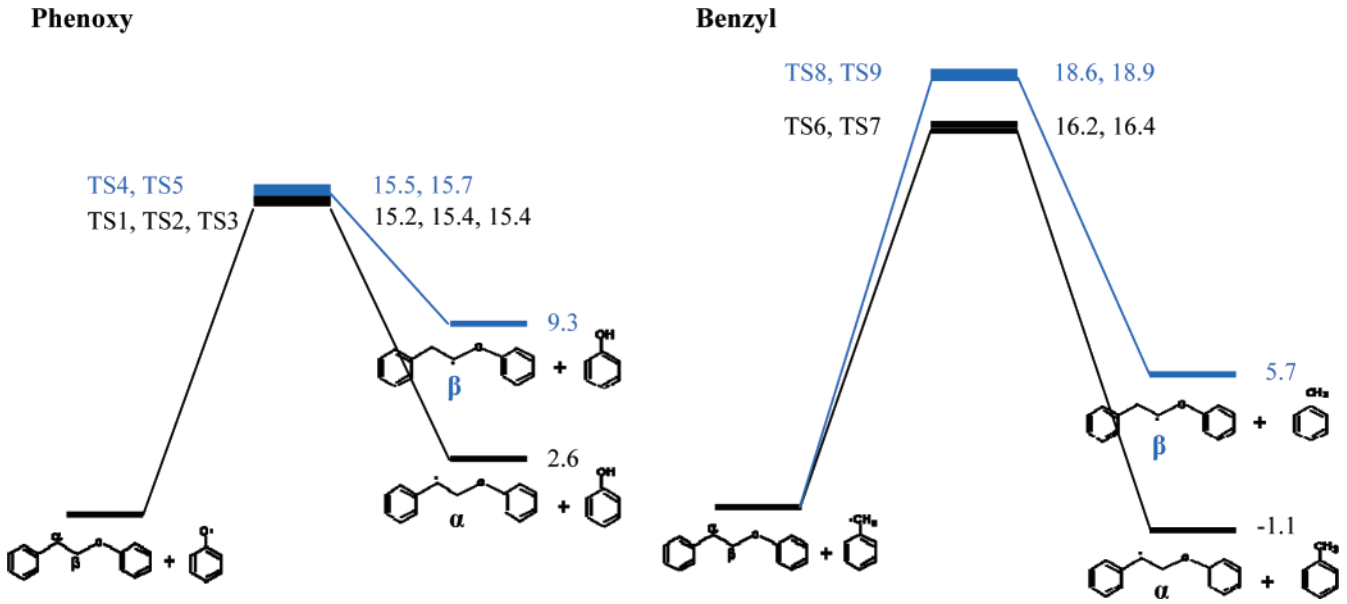

Figure 5. Reaction profile for the hydrogen abstraction on PPE by phenoxyl radical (reaction 2) and benzyl radical (reaction 6); energy differences in kcal/mol.

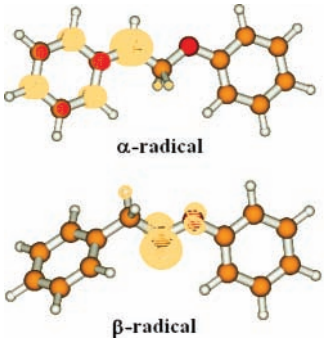

Figure 6. Spin densities for the α- and β-radical of PPE.

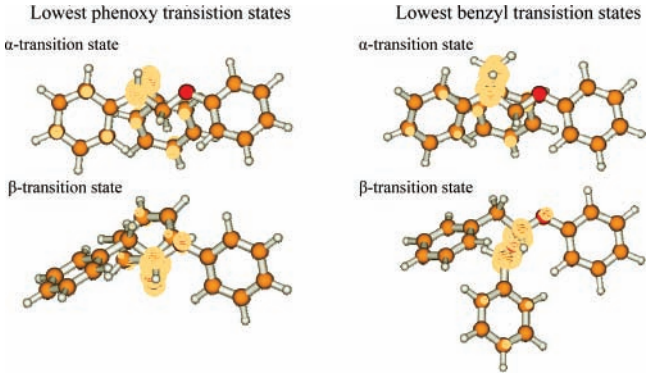

Figure 7. Spin densities for the lowest transition states of the hydrogen abstraction reactions on PPE by the phenoxyl radical (reaction 2) and the benzyl radical (reaction 6).

computed an approximate anharmonic potential as follows. We performed two additional single point calculations with geometries displaced along the normal mode. The anharmonic potential was assumed to have the form of a polynomial including second-, third-, and fourth-order terms. The second-order force constant was taken from the harmonic calculation. We solved for the third- and fourth-order force constants using the energies obtained from the single point calculations. The semiclassical partition functions were computed as described above. For all frequencies above 100 cm^{-1} we applied the quantum harmonic approximation for the partition function. We checked the validity of the approximate potential for a frequency in **TS2** of 19.7 cm^{-1}, which is close to our chosen value of 20 cm^{-1} for the transition between full and approximate potential. The semiclassical partition function calculated with the full potential at 648 K is 8.40, the semiclassical partition function calculated with the approximate potential is 8.36.

To calculate the α/β-selectivity, we only need the activation barriers and partition functions of the transition states. However, for a consistency check, we also calculated the overall activation energies and prefactors for each reaction. To obtain these, we needed the partition functions of the reactants as well. The benzyl and phenoxyl radicals do not have frequency modes below 100 cm^{-1} and the quantum harmonic approximations were used for all vibrational partition functions. PPE has four harmonic frequencies smaller than 100 cm^{-1} for which the semiclassical expression for the partition function was applied and for which we computed approximate anharmonic potentials using the harmonic second-order force constant and performing two additional single-point calculations to obtain the higher-order terms. Again, for frequencies above 100 cm^{-1} the harmonic quantum partition function was employed.

In general, the semiclassical approximation is applicable in the limit of high temperatures and low frequencies. To verify the applicability within the parameter set of our calculations, we chose the highest harmonic frequency and the lowest temperature for which we apply the semiclassical approximation in **TS1** (104.5 cm^{-1} at 600 K) and calculated the quantum partition function using the same anharmonic potential. The semiclassical partition function is calculated to be 3.40 and the quantum partition function is computed to be 3.40 as well; however, the calculation of the semiclassical partition function is significantly faster.

In Table 1 we demonstrate the large impact on the partition functions when an anharmonic potential is used for **TS4** at 648 K. (We chose a transition state with only one imaginary mode to be able to calculate the harmonic quantum partition function for comparison.) Table 1 also shows that the anharmonic and harmonic partition functions become increasingly similar the higher the frequency, indicating that the harmonic partition function is sufficiently accurate above 100 cm^{-1}.

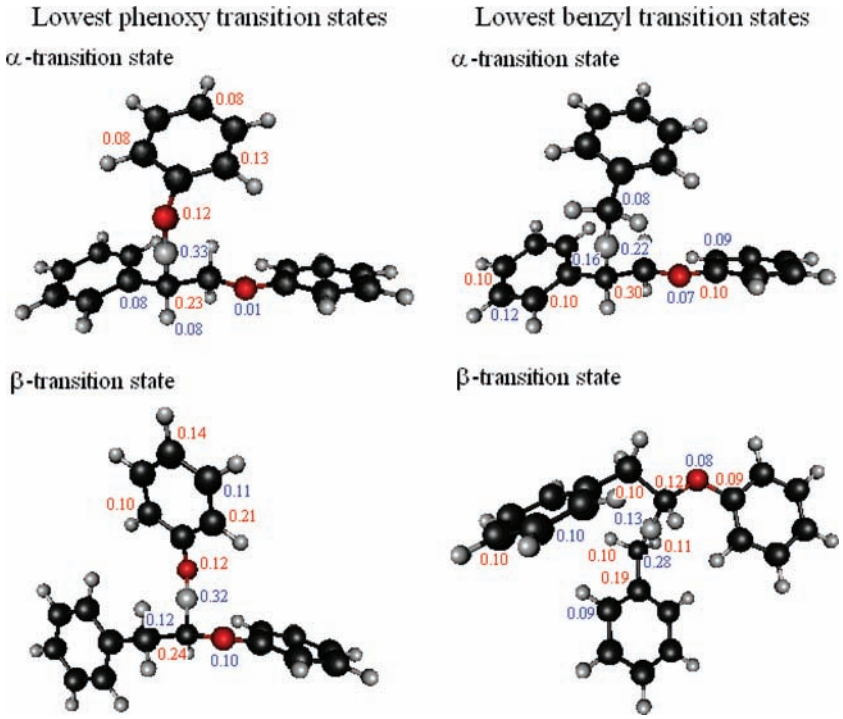

Figure 8. Charge differences [in electrons] between the transition states and the reactants for the lowest transition states of the α- and *β*-pathways for phenoxyl (reaction 2) and benzyl abstraction (reaction 6): red, charge gain; blue, charge loss; display cutoff 0.08 e^- except for the ether oxygen, which is always monitored.

TABLE 1: Harmonic Quantum q_v^Q and Anharmonic Semiclassical q_v^{SC} vibrational Partition Functions for TS4 at $T = 648$ K

ν (cm^{-1})	13.9	27.8	32.3	40.6	50.8	53.5	62.7	68.5	102.2
q_v^Q	32.8	16.7	14.4	11.6	9.4	8.9	7.7	7.1	4.9
q_v^{SC}	8.6	10.3	6.6	6.1	8.8	5.4	6.8	6.1	4.2

At this point we make a short assessment of the accuracy of the diagonal anharmonic corrections in the low-frequency modes. We have shown that the spurious imaginary modes have large fourth-order contributions. On the other hand, we have demonstrated that the harmonic approximation above 100 cm^{-1} is appropriate and we have seen that between 20 and 100 cm^{-1} the approximate potential works well. Because the approximate potential uses the harmonic force constant, the harmonic approximation is correct to first-order. Coupling between modes is included within the harmonic approximation, which seems reasonable because only for the lowest mode the harmonic approximation breaks down completely.

We calculated the rate constants for the hydrogen abstraction on PPE by the phenoxyl radical (reaction 2) and by the benzyl radical (reaction 6) for the experimental temperature range 600−700 K and plotted ln *k* as a function of 1/*T* in Figure 9. The overall activation energies and prefactors obtained from the plots are summarized in Table 2. The experimental values in Table 2 are estimates but demonstrate that our calculated values are of the same order. The experimental Arrhenius values are obtained from experimental data on related reactions combined with thermochemical kinetic analysis employing group additivity, as described in ref 13.[13b]

The anharmonic corrections have a large influence on the total rate constant: when the harmonic partition functions are used for all the frequencies in the transition states and reactants, the rate constant for reaction 2b is 235 L mol^{-1} s^{-1}; when the partition functions of the lower frequencies incorporate anharmonic corrections, the rate constant changes to 28.3 L mol^{-1} s^{-1}. Table 2 also includes the calculated activation energies and prefactors (when possible) when no anharmonic corrections are applied. We observe that the anharmonic corrections lower the prefactors and activation energies, both resulting in the decrease of the rate constant. However, the changes are not constant, which impacts the relative rate constant. At 648 K the α/*β*-selectivity for the benzyl abstraction is calculated to be 6.4; the α/*β*-selectivity computed without anharmonic corrections in the low-frequency partition functions is 30.5.

In Table 3 the α/*β*-selectivities for the hydrogen abstraction on PPE by the phenoxyl radical and by the benzyl radical in the experimental temperature range are given. With increasing temperature the α/*β*-selectivities decrease because the energetically higher *β*-pathways gain more influence. The α/*β*-selectivity of the hydrogen abstraction by the benzyl radical, which has a larger barrier difference, has a stronger temperature dependence.

The overall α/*β*-selectivity has been measured to be 3.1 ± 0.3 at 648 K.[13] We can derive an expression for the overall α/*β*-selectivity invoking the quasi-steady-state approximation,[58] where the assumption is made that all radical and intermediate concentrations are negligible compared to those of reactants and products, which is reasonable because the intermediate radicals in Scheme 1 are short-lived. We also assume that the interconversion between the α- and *β*-radical (**1** and **2** in Scheme 1) is slow, which is based on the experimental evidence.[13] According to Scheme 1 all α-abstraction yields phenoxyl radicals that abstract hydrogen from PPE, producing phenol. All *β*-abstraction yields benzyl radicals that abstract hydrogen producing toluene. The overall α/*β*-selectivity is therefore given as the rate of formation of phenol divided by the rate of formation of toluene. Applying the quasi-steady-state approximation for the radical intermediates involved leads to

$$\frac{d[PhOH]/dt}{d[PhCH_3]/dt} = \frac{y}{1-x} \qquad (10)$$

y is the fraction of reactants following the α-pathway in the hydrogen abstraction by the benzyl radical (reaction 6a), with

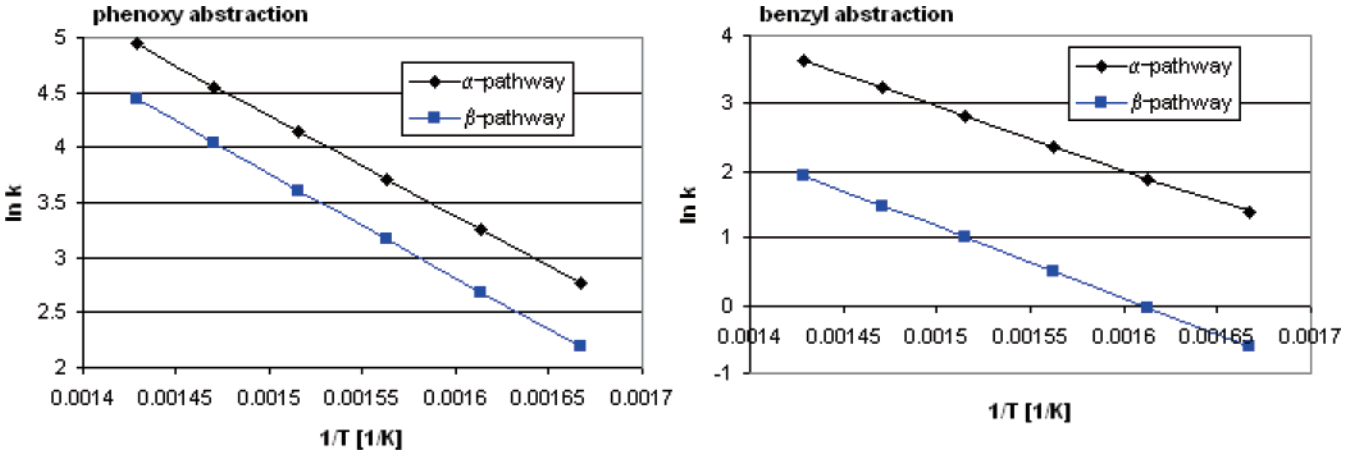

Figure 9. Arrhenius plots for the computed rate constants of the α- and β-pathways of the hydrogen abstraction on PPE by the phenoxyl radical (reaction 2) and the benzyl radical (reaction 6).

TABLE 2: Prefactors and Activation Energies Obtained from the Arrhenius Plots for the Hydrogen Abstraction Reactions on PPE by the Phenoxyl Radical (Reaction 2) and the Benzyl Radical (Reaction 6)[a]

		calcd		exp[13b]	
		ln *A*	E_a (kcal/mol)	ln *A*	E_a (kcal/mol)
phenoxyl	α	18.0	18.2		
(reaction 2)	β	17.9 (20.6)	18.8 (19.5)		
benzyl	α	17.2 (22.4)	18.8 (19.9)	19.1	14.4
(reaction 6)	β	17.2 (20.8)	21.2 (22.3)	19.6	17.6

[a] Experimental estimates from ref 13. Temperature range 600−700 K. Values in parentheses are obtained by using quantum vibrational partition functions only.

TABLE 3: α/β-Selectivities for the Hydrogen Abstraction on PPE by the Phenoxyl and by the Benzyl Radical at Different Temperatures

	α/β-selectivity on PPE					
	600 K	620 K	640 K	660 K	680 K	700 K
phenoxyl radical	1.78	1.75	1.73	1.70	1.68	1.66
benzyl radical	7.43	6.96	6.55	6.18	5.86	5.56

$(1 - y)$ being the fraction of the reactants following the β-pathway (reaction 6b). x is the fraction of reactants following the α-pathway in the hydrogen abstraction by the phenoxyl radical (reaction 2a), with $(1 - x)$ being the fraction of the reactants following the β-pathway (reaction 2b). We have calculated the α/β-selectivity for the hydrogen abstraction reaction by the phenoxyl radical $x/(1 - x) = 1.72$ at 648 K and the α/β-selectivity for the hydrogen abstraction reaction by the benzyl radical $y/(1 - y) = 6.40$ at 648 K, from which we obtain an overall α/β-selectivity of 2.35 at 648 K for the hydrogen abstraction on PPE according to eq 10. This calculated overall α/β-selectivity is in very good agreement with the experimental value of 3.1 ± 0.3 at 648 K, in particular, considering the assumptions involved.

Conclusion

We have shown that the overall α/β-selectivity can be predicted for hydrogen abstraction reactions occurring in the thermal decomposition of model compounds for the β-ether linkage in lignin. The calculation of the α/β-selectivity of an individual reaction benefits from the fact that the relative rate constant depends only on the reaction barriers and pre-factors of similar transition states; i.e., the reactants are the same. Error cancellation is effective for the reaction barriers. Because the rate constants are extremely sensitive to the values of the vibrational partition functions of the low-frequency modes that have large anharmonic contributions, error cancellation is less effective for the pre-factors within a harmonic approximation. The transition states of the hydrogen abstraction reactions on PPE have a large number of low-frequency modes (nine frequencies per transition states have harmonic frequencies under 100 cm^{-1}).

We propose a scheme for the calculation of relative rate constants where we use the B3LYP functional in combination with transition-state theory. We apply diagonal anharmonic corrections to calculate the vibrational partition functions of low-frequency modes. The anharmonic potentials up to fourth-order are obtained by fitting the potential retrieved from single point calculations at displaced geometries along the normal mode to a polynomial. The anharmonic potentials are then used in a semiclassical expression for the vibrational partition function based on a second-order Wigner−Kirkwood expansion. The calculated relative rate constants are used in a kinetic analysis that uses quasi-steady-state conditions for the radical intermediates in the pyrolysis of PPE. The calculated overall α/β-selectivity of 2.4 at 648 K is in very good agreement to the experimental value of 3.1 ± 0.3 at 648 K.

We analyzed the electronic structure of the transition states to explain energy barrier differences between the hydrogen abstraction reactions on PPE by the benzyl radical and by the phenoxyl radical. The α-transition states are stabilized by electron delocalization into the adjacent aromatic ring, which does not occur for the β-transition states. If the abstracting radical is strongly electrophilic, as in the case of phenoxyl, the β-transition state is stabilized by charge donation from the adjacent ether oxygen in PPE. These two opposing effects cause the reaction barriers for the α- and β-pathways for the hydrogen abstraction by phenoxyl to be similar. The benzyl radical lacks the ability to withdraw charge from PPE and the β-transition state is not stabilized by the ether oxygen. Consequently, the energy barrier difference for the α- and β-pathways for the hydrogen abstraction by the benzyl radical is larger.

On the basis of the work presented, we will be able to study substituent effects in the pyrolysis of model compounds for the β-ether linkage in lignin, predict α/β-selectivities, and explain the underlying differences between the α- and β-pathways by characterizing the electronic structure of the transition states.

Acknowledgment. This research was supported by the Division of Chemical Sciences, Geosciences, and Biosciences,

Office of Basic Energy Sciences, U.S. Department of Energy, under contract DE-AC05-00OR22725 with Oak Ridge National Laboratory, managed and operated by UT-Battelle, LLC, and in part by ORNL Laboratory Directed Research and Development Funds. This research was performed in part using the resources of the Center for Computational Sciences at Oak Ridge National Laboratory under contract DE-AC05-00OR22725. This document describes activities performed under contract number DE-AC0500OR22750 between the U.S. Department of Energy and Oak Ridge Associated Universities.

References and Notes

(1) Fushimi, C.; Araki, K.; Yamaguchi, Y.; Tsutsumi, A. *Ind. Eng. Chem. Res.* **2003**, *42*, 3929.

(2) Ferdous, D.; Dalai, A. K.; Bej, S. K.; Thring, R. W. *Energy Fuels* **2002**, *16*, 1405.

(3) Bocchini, P.; Galletti, G. C.; Camarero, S.; Martinez, A. T. *J. Chromatogr.* **1997**, *773*, 227.

(4) Mohan, D.; Pittman, C. U., Jr.; Steele, P. H. *Energy Fuels* **2006**, *20*, 848.

(5) Huber, G. W.; Iborra, S.; Corma, A. *Chem. Rev.* **2006**, *106*, 4044.

(6) Amen-Chen, C.; Pakdel, H.; Roy, C. *Bioresour. Technol.* **2001**, *79*, 277.

(7) Dorrestijn, E.; Laarhoven, L. J. J.; Arends, I. W. C. E.; Mulder, P. *J. Anal. Appl. Pyrol.* **2000**, *54*, 153.

(8) McDermott, J. B.; Klein, M. T.; Obst, J. R. *Ind. Eng. Chem. Process Des. Dev.* **1986**, *25*, 885.

(9) Kuroda, K. J. *Anal. Appl. Pyrolysis* **1994**, *30*, 173. Kuroda, K. J. *Anal. Appl. Pyrol.* **1995**, *35*, 53. Kuroda, K.; Nakagawa-izumi, A. *Org. Geochem.* **2006**, *37*, 665.

(10) Britt, P. F.; Buchanan, A. C., III; Cooney, M. J.; Martineau, D. R. *J. Org. Chem.* **2000**, *65*, 1376.

(11) Drage, T. C.; Vane, C. H.; Abbott, G. D. *Org. Geochem.* **2002**, *33*, 1523.

(12) Kandanarachi, P. H.; Autrey, T.; Franz, J. A. *J. Org. Chem.* **2002**, *67*, 7937.

(13) (a) Britt, P. F.; Buchanan, A. C., III; Malcolm, E. A. *J. Org. Chem.* **1995**, *60*, 6523. (b) The best experimental rate constant for a reference reaction (2-allylbenzyl radical abstracting hydrogen from *m*-xylene: Franz; et.al. *J. Org. Chem*. **1986**, *51*, 1446) has an error of 0.7 kcal/mol in the activation energy and 0.4 in log *A*. The group additivity parameters (from Benson's book, ref 58 in ref 13) have errors associated with them also. An overall estimate of the errors in the experimental values is 1−2 kcal/mol for the activation energies and 2.5 for ln *A*.

(14) Klein, M. T.; Virk, P. S. *Ind. Eng. Chem. Fundam.* **1983**, *22*, 35.

(15) Gilbert, K. E.; Gajewski, J. J. *J. Org. Chem.* **1982**, *47* 4899. Gilbert, K. E. *J. Org. Chem.* **1984**, *49*, 6.

(16) Chen, X.; Zhang, X.; Han, K.; Varandas, A. J. C. *Chem. Phys. Lett.* **2006**, *421*, 453.

(17) Wang, W.; Feng, L.; Wang, W.; Luo, Q.; Li, Q. *J. Mol. Struct. (THEOCHEM)* **2006**, *764*, 53.

(18) Phillips, D. L.; Zhao, C.; Wang, D. *J. Phys. Chem. A* **2005**, *109*, 9653.

(19) Zhang, Y.; Li, Q. S.; Zhang, S. *J. Mol. Struct. (THEOCHEM)* **2004**, *682*, 163.

(20) Chan, W.-T.; Hamilton, I. P.; Pritchard, H. O. *J. Chem. Soc., Faraday Trans.* **1998**, *19*, 2303.

(21) González-Lafont, À.; Lluch, J. *J. Mol. Struct. (THEOCHEM)* **2004**, *709*, 35.

(22) Wang, C.; Zhang, Y.; Zhang, S.; Li, Q. S. *Theor. Chem. Acc.* **2006**, *115*, 205.

(23) Wang, Y.; Liu, J.-Y.; Li, Z.-S.; Wang, L.; Wu, J.-Y.; Sun, C.-C. *Chem. Phys.* **2006**, *324*, 609.

(24) Zhang, Q.; Wang, H.; Sun, T.; Wang, W. *Chem. Phys.* **2006**, *324*, 298.

(25) Sun, H.; He, H.; Gong, H.; Pan, X.; Li, Z.; Wang, R. *Chem. Phys.* **2006**, *327*, 91.

(26) Garrett, B. C.; Truhlar, D. G. *J. Chem. Phys.* **1979**, *70*, 1593.

(27) Garrett, B. C.; Truhlar, D. G. *J. Am. Chem.* **1979**, *101*, 4534.

(28) Hemelsoet, K.; Speybroeck, V. V.; Moran, D.; Marin, G. B.; Radom, L.; Waroquier, M. *J. Chem. Phys. A* **2006**, *110*, 13624.

(29) Violi, A.; Truong, T. N.; Sarofim, A. F. *J. Chem. Phys. A* **2004**, *108*, 4846. Chae, K.; Violi, A. *J. Org. Chem.* **2007**, *72*, 3179.

(30) Leininger, J.-P.; Minot, C.; Lorant, F.; Behar, F. *J. Phys. Chem. A* **2007**, *111*, 3082.

(31) Hemelsoet, K.; Moran, D.; Speybroeck, V. V.; Waroquier, M.; Radom, L. *J. Chem. Phys. A* **2006**, *110*, 8942.

(32) Allen, W. D.; Bodi, A.; Szalay, V.; Császár, A. G. *J. Chem. Phys.* **2006**, *124*, 224310.

(33) Beste, A.; Buchanan, A. C., III; Britt, P. F.; Hathorn, B. C.; Harrison, R. J. To be published.

(34) Willetts, A.; Handy, N. C.; Green, W. H., Jr.; Jayatilaka, D. *J. Phys. Chem.* **1990**, *94*, 5608.

(35) Gregurick, S. K.; Chaban, G. M.; Gerber, R. B. *J. Phys. Chem. A* **2002**, *106*, 8696.

(36) Christiansen, O. *J. Chem. Phys.* **2003**, *119*, 5773.

(37) Schneider, W.; Thiel, W. *Chem. Phys. Lett.* **1989**, *157*, 367. Dressler, S.; Thiel, W. *Chem. Phys. Lett.* **1997**, *273*, 71.

(38) Ruden, T. A.; Taylor, P. R.; Helgaker, T. *J. Chem. Phys.* **2003**, *119*, 1951.

(39) Neugebauer, J.; Hess, B. A. *J. Chem. Phys.* **2003**, *118*, 7215.

(40) Barone, V. *J. Chem. Phys.* **2004**, *120*, 3059.

(41) Wigner, E. P. *Phys. Rev.* **1932**, *40*, 749. Kirkwood, J. G. *Phys. Rev.* **1933**, *44*, 31.

(42) McQuarrie, D. A. *Statistical Mechanics*; University Science Books: Sausalito, CA, 2000.

(43) Apra, E. et al. *NWChem, A Computational Chemistry Package for Parallel Computers, Version 4.7*; Pacific Northwest National Laboratory: Richland, WA 99352−0999, 2005.

(44) Becke, A. D. *J. Chem. Phys.* **1993**, *98*, 5648.

(45) Lee, C.; Yang, W.; Parr, R. G. *Phys. Rev. B* **1988**, *37*, 785.

(46) Temelso, B.; Sherrill, C. D.; Merkle, R. C.; Freitas, R. A., Jr. *J. Phys. Chem. A* **2006**, *110*, 11160.

(47) Patchkovskii, S.; Ziegler, T. *J. Chem. Phys.* **2002**, *116*, 7806.

(48) Pickard, F. C., IV; Shepherd, R. L.; Gillis, A. E.; Dunn, M. E.; Feldgus, S.; Kirschner, K. N.; Shields, G. C.; Manoharan, M.; Alabugin, I. V. *J. Phys. Chem. A* **2006**, *110*, 2517.

(49) Wang, Z. G.; Pan, S. F.; Yao, M. G.; Wang, G.; Lv, S. W.; Yang, J.; Jin, M. X.; Li, W. Q. *J. Mol. Struct. (THEOCHEM)* **2006**, *767*, 95.

(50) De Lucas, N. C.; Correa, R. J.; Albuquerque, A. C. C.; Firme, C. L.; Garden, S. J.; Bertoti, A. R.; Netto-Ferreira, J. C. *J. Phys. Chem. A* **2007**, *111*, 1117.

(51) Becke, A. D. *J. Chem. Phys.* **1993**, *98*, 1372.

(52) Zhang, Q.; Bell, R.; Truong, T. N. *J. Chem. Phys.* **1995**, *99*, 592.

(53) Durant, J. L. *Chem. Phys. Lett.* **1996**, *256*, 595.

(54) Lynch, B. J.; Fast, P. L.; Harris, M.; Truhlar, D. G. *J. Phys. Chem. A* **2000**, *104*, 4811.

(55) Lynch, B. J.; Truhlar, D. G. *J. Phys. Chem. A* **2001**, *105*, 2936.

(56) Coote, M. L. *J. Phys. Chem. A* **2004**, *108*, 3865.

(57) Kochi, J. K., Ed. *Free Radicals*; John Wiley & Sons, Inc.: New York, NY, 1973; Vol. I.

(58) Benson, W. S. *Thermochemical Kinetics*, 2nd ed.; John Wiley & Sons, Inc.: New York, NY, 1976.